Porosity Detection by Computed Tomography

Grzegorz Ziółkowski, Patrycja Szymczyk, Andrzej Pawlak, Tomasz Kurzynowski, Bogdan Dybała, Edward Chlebus
Wrocław University of Science and Technology, Faculty of Mechanical Engineering, Centre for Advanced Manufacturing Technologies (CAMT-FPC), Łukasiewicza 5, 50-371 Wrocław, Poland

Abstract: Industrial computed tomography (CT) supports quality inspection of manufactured technical objects and product development thanks to its possibility of non-destructive detection of porosity. Application of computed tomography to porosity detection permits not only qualitative evaluation of internal structure of objects, but also quantitative evaluation of material porosity with representation of three-dimensional shape of pores and their spatial distribution. The paper presents a brief characteristic of the factors influencing effectiveness of porosity detection by CT. A technical example illustrates influence of the applied magnification on the possibility to detect porosity and represent shapes of pores. Next, the results of porosity evaluation obtained by CT and by standard microscopic examinations are compared. It was demonstrated that result of porosity detection is influenced by magnification and resolution of CT measurements.

Keywords: technical computed tomography, porosity, defectoscopy, quality inspection

1. Introduction

An industrial CT scanner is equipped with an X-ray tube generating a conical beam of radiation. It can be used for representing external and internal geometry of technical objects. After CT examination, structure of the object remains unchanged, so this technique is classified as a non-destructive testing [1–4]. By CT it is possible to analyse internal structure of examined objects in a relatively short time, with no need of their expensive cutting into sections. Schematic presentation of obtaining three-dimensional data using CT is shown in Fig. 1.

During reconstruction, the object is placed on a turntable and screened with X-rays. The object is penetrated by radiation at various angular positions of the table and a series of X-ray images is recorded. Based of these digitally recorded images composed of individual pixels with various intensities, a 3D model of the scene is reconstructed. The object is separated from the background by segmentation using the thresholding technique and, finally, a 3D model of the object itself is created.
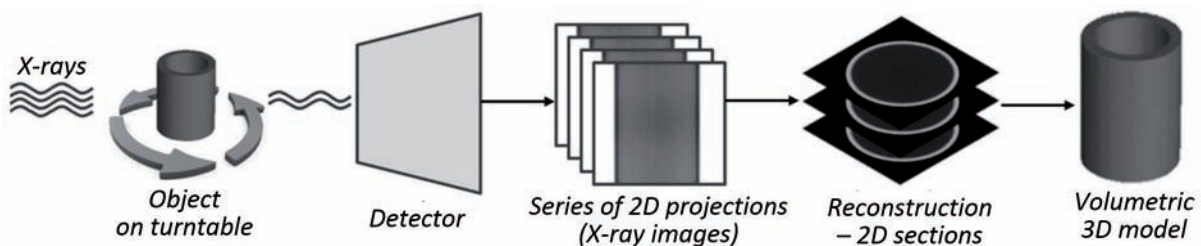

Fig. 1. Schematic presentation of obtaining data by technical CT
Rys. 1. Schemat uzyskiwania danych z wykorzystaniem technicznej tomografii komputerowej

Autor korespondujący:
Patrycja Szymczyk, patrycja.e.szymczyk@pwr.edu.pl

A map representing 3D geometry, obtained by CT reconstruction, makes it possible to detect hidden material defects in form of pores, cracks, inclusions and other discontinuities inside the reconstructed objects [5–7], see Fig. 2. An advantage of this measurement method is quantitative analysis of defects that makes it possible to evaluate total porosity with determination of shapes of pores and their spatial distribution. However, the possibility of detecting pores by CT depends on many
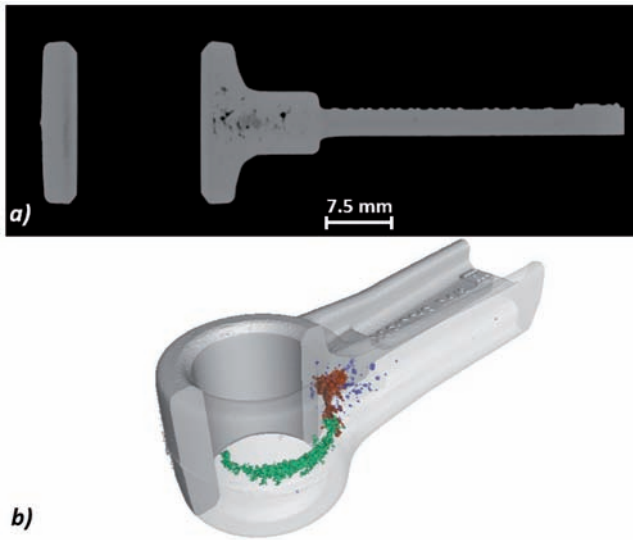
Fig. 2. Reconstruction of an aluminum part: a) result of reconstruction in form of 2D section recorded in grey scale; b) 3D view after segmentation of data, pores are marked with various colours
Rys. 2. Rekonstrukcja aluminiowego detalu: a) wynik rekonstrukcji w postaci przekroju 2D zapisanego w skali szarości, b) widok 3D po segmentacji danych i zaznaczeniu porów różnymi kolorami
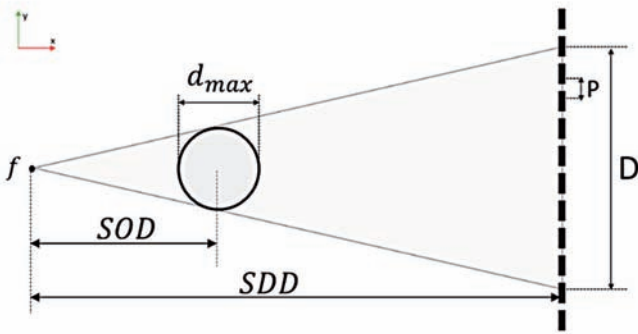

Fig. 3. Operating principle of a technical CT scanner with a conical X-ray beam
Rys. 3. Schemat ideowy tomografu technicznego ze stożkową wiązką promieniowania

factors; the most important of them will be described below in more details.

Detection of porosity using CT is limited by size of the reconstructed object that determines the attainable measurement resolution [8]. Maximum size of the object to be reconstructed dmax restricts possible magnifications, which results from geometrical relationships of the CT measuring system, see Fig. 3. Magnification m can be expressed by the formula:

$$m = \frac{SDD}{SOD}, \tag{1}$$

where SDD is the source-to-detector distance and SOD is source-to-object distance.

The possible magnification is also expressed by the ratio between the detector size D and maximum dimension of the reconstructed object d_{max}, according to the relationship:

$$m = \frac{D}{d_{max}}. \tag{2}$$

Spatial resolution in computed tomography is directly linked to the idea of "voxel", i.e. a three-dimensional cubic element corresponding to a pixel of the 2D system. The CT reconstruction is a three-dimensional matrix of such elements and each of them has a determined intensity in grey scale, corresponding to "density" (attenuation of X-rays) of the represented piece of material in the reconstructed object, see Fig. 4. Summarising, the size of a voxel V_X is proportional to the largest dimension of the reconstructed object d_{max} and magnification m and depends on sizes of the detector D and the detector pixel P. So, size of a voxel can be expressed as follows:

$$V_x = \frac{P}{m} \quad \Rightarrow \quad V_x = \frac{d_{max} \cdot P}{D}. \tag{3}$$

The relation (3) determines size of a voxel, limited by maximum dimension of the object. The smaller size of a voxel, the smaller defects can be recorded and, thus, porosity recorded for a smaller voxel by CT is more accurate (better resolution) [9]. Discretisation of an object in form of voxel data is not free of shortcomings, as schematically shown in Fig. 5. The partial volume effect (PVE) [10] occurs here, limiting or precluding
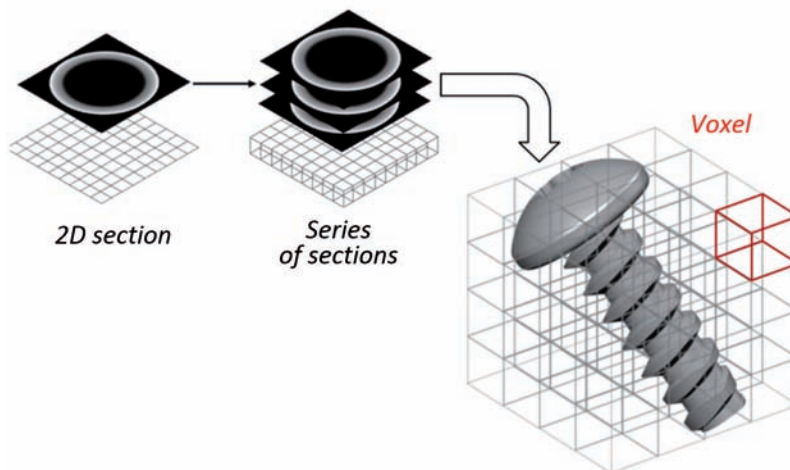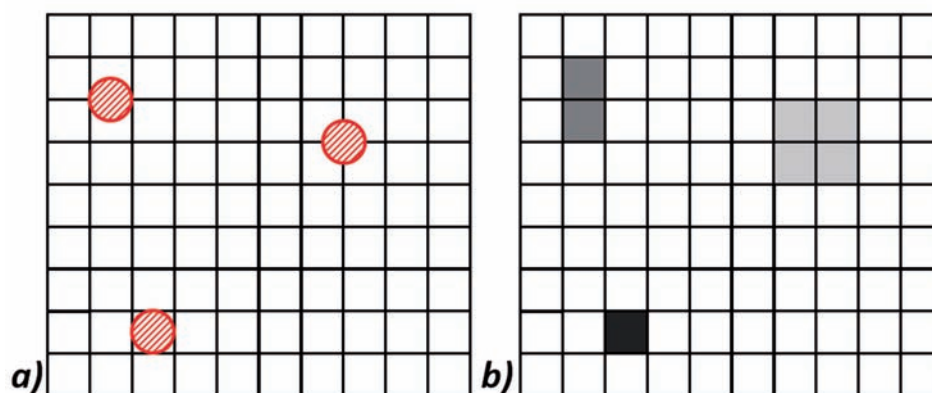

Fig. 4. Schematic presentation of a voxel as a three-dimensional element corresponding to a pixel from the 2D system
Rys. 4. Schematyczne przedstawienie woksela jako trójwymiarowego elementu odpowiadającego pikselowi z układu 2D

Fig. 5. Schematic presentation of PVE: a) real porosity shown in 2D; b) porosity recorded in form of voxels
Rys. 5. Schematyczne przedstawienie PVE: a) porowatość rzeczywista pokazana w 2D; b) zarejestrowana porowatość w formie wokseli

detection of small pores. The PVE effect results in incorrect recording of grey scale and this, in turn, causes that the recorded shape of pores depends on the relation of voxel size to the size of the represented inhomogeneity.

Porosity detection is also restricted by measurement artefacts, whose intensity increases with the density of the reconstructed object. Such artefacts include beam hardening [11] that is revealed in form of non-homogeneous grey scale recorded for a homogeneous material, or X-ray scattering resulting in significant quality reduction of reconstruction [12]. Additional factors significantly affecting possibility of porosity detection are related to segmentation of voxel data [13] or to the used detection algorithm [14].

2. Method

In the examinations, a reference sample of titanium alloy Ti6Al7Nb (density 4.52 g/cm³) manufactured by selective laser melting (SLM) was used. The sample was composed of six cylinders stacked on one another, making a stepwise cone. Diameters of the cylinders ranged between 10 mm and 35 mm and total height of the sample was 15 mm, see Fig. 6a.

The sample was reconstructed six times by a CT system Zeiss Metrotom 1500, equipped with an X-ray tube with minimum focal spot 7 µm and maximum accelerating voltage 225 kV. The system contained a 16-bit amorphous silicon flat-panel detector with 1024 × 1024 pixel matrix (physical size of a pixel was 400 µm). The SDD value was 1501 mm. Reconstruction was carried-out with voltage of the X-ray tube equal to 225 kV, integration time of the detector 2 s, copper filter 0.5 mm thick, and with 1050 projections. In order to demonstrate the influence of the applied magnification on porosity detection, reconstruction was limited to the first step of the sample (Fig. 6a), which made it possible to take measurements with voxel size from 15 µm to 65 µm, see Table 1.

Table 1. Measurement parameters used in the experiment
Tabela 1. Parametry pomiaru wykorzystane w eksperymencie

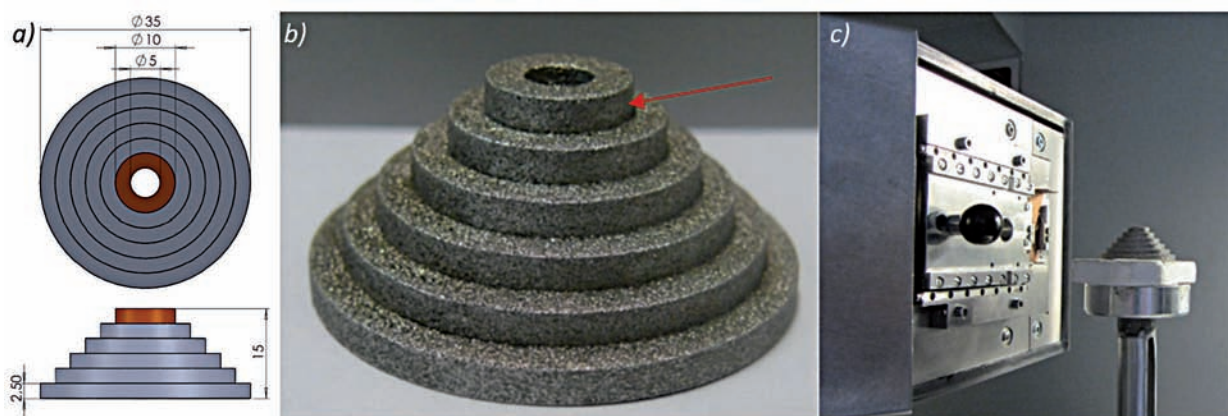| No. of reconstruction	1	2	3	4	5	6
Magnification (m)	26.6×	20×	13.3×	10×	8×	6.2×
Voxel size (V_x)	15 µm	20 µm	30 µm	40 µm	50 µm	65 µm

Fig. 6. Sample made by SLM from titanium alloy Ti6Al7Nb. The smallest step of the sample (marked brown) was reconstructed: a) dimensions of the sample; b) view of the sample; c) object in the measurement chamber of the CT system
Rys. 6. Wzorzec wytworzony w technologii SLM ze stopu tytanu Ti6Al7Nb. Rekonstrukcji poddano najmniejszy stopień wzorca (zaznaczony kolorem):
a) wymiary wzorca, b) wytworzony wzorzec, c) obiekt w komorze pomiarowej systemu CT
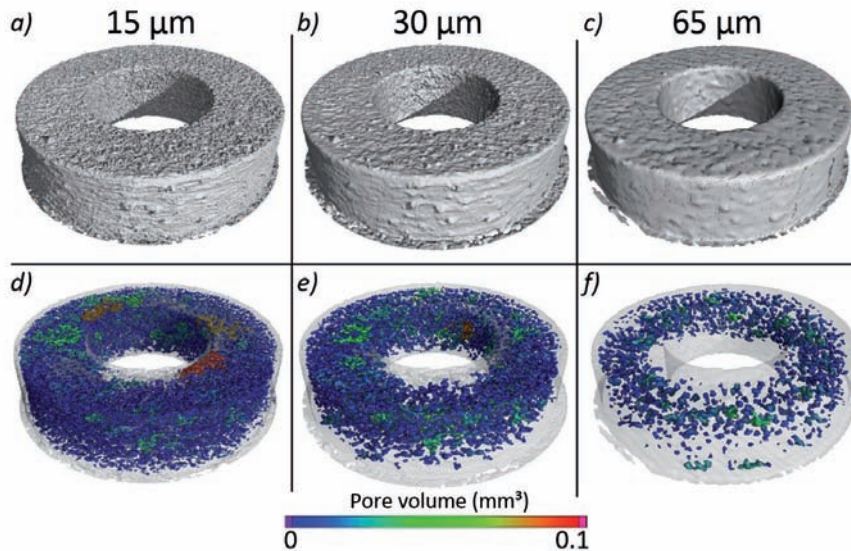
Fig. 7. Three-dimensional CT reconstructions of Ti sample made with various voxel sizes, showing internal shape and recorded porosity
Rys. 7. Trójwymiarowe rekonstrukcje CT tytanowego wzorca wykonane z różną wielkością woksela, przedstawiające kształt zewnętrzny i zarejestrowaną porowatość wnętrza

After performing reconstructions with six magnification levels, volumetric porosity P_V for each reconstruction was determined according to the relationship:

$$P_V = \frac{V_p}{V_p + V_m} \quad [\%], \tag{4}$$

where V_p is volume of pores and V_m is volume of the material.

Porosity was detected using the software Volume Graphics VG Studio 2.0. The "Enhanced" algorithm was used with the following parameters: pore size above 8 voxel, probability threshold 1.0.

3. Results

Exemplary visualisations of external geometry and porosity inside the object reconstructed with various voxel sizes are shown in Fig. 7.

In the case of a reconstruction with the maximum magnification, external geometry of the object is visible in details (Fig. 7a) and the recorded porosity is the biggest because many small pores are detected, see Fig. 7d. For the magnification corresponding to 30 µm voxels, the outside surface is smoothed, with smaller number of registered details, see Figs. 7b and 7e. For the reconstruction with 65 µm voxels, details in form of unmelted powder grains (a feature of the additive technology SLM, where powder particles are stuck to the molten pool at the boundary of molten material) present on surface of the object are not completely represented, see Fig. 7c. Comparison of porosity values recorded at various magnifications is shown in Fig. 8. Porosity recorded for 15 µm voxels was 8.33%. When voxel size was increased to 30 µm, the recorded porosity slightly changed to about 8%. For reconstruction with 40 µm voxels, porosity was significantly lower at 7.02%. For reconstruction with 65 µm voxels, recorded porosity level was less than half of that reconstructed for 15 µm voxels, i.e. about 4%.

In order to express porosities for reconstructions with various voxel sizes in qualitative way, a coefficient determining sphericity of pores, calculated as the ratio of a pore volume V to its surface area A, was calculated according to the formula:

$$S = \frac{\pi^{1/3}(6V)^{2/3}}{A}, \tag{5}$$

where $S \in [0, 1]$.

For an ideal sphere, the sphericity coefficient S = 1 [15]. Results in form of histograms showing numbers of pores with various sphericity coefficients are given in Fig. 9. At larger voxel sizes, numbers of recorded pores are smaller, which can be clearly seen by comparison of the histograms obtained for 15 µm (blue) and 65 µm (red) voxels. For larger voxels, larger numbers of pores with higher sphericity coefficients were recorded. The histograms for larger voxels are located closer to the sphericity coefficient equal to 1, which means spherical shape of pores. This also means that pores recorded at lower magnifications (with larger voxels) are recorded with less exactly represented shape.

Results of porosity measurements using CT were verified by comparison with results of standard microscopic observations on a polished cross-section, see Fig. 10. Comparison was carried out for the reconstruction with the highest magnification, since the expected results for this magnification would be closest to the real values. After all the reconstructions were completed, the first stage of the examined sample was cut horizontally and polished to visualise internal structure of the examined cross-section. The image of the metallographic section was recorded with a confocal microscope OLYMPUS 3D LEXT OLS4000 at magnification 140×.

The so obtained image was subjected to binarization by the software *ImageJ* and surface porosity P_A on a plane of the test piece was determined from the formula:

$$P_A = \frac{A_p}{A_p + A_m} \quad [\%], \tag{5}$$

where A_p means the surface of pores and A_m means the surface sample of the sample.

In order to compare the results, the section of CT reconstruction, corresponding to the plane of the metallographic section, was determined. That section was also subjected to binarization and surface porosity was determined. This way, porosities determined on the same section for tomographic and
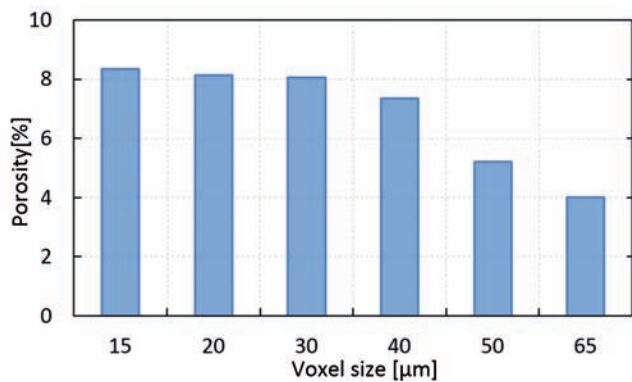
Fig. 8. Volumetric porosity measured for the examined sample
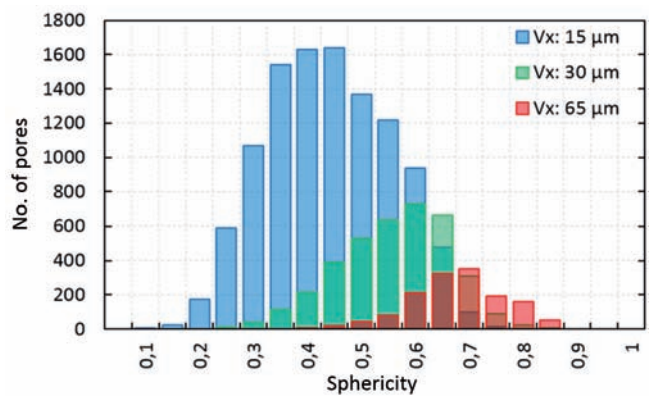Rys. 8. Wyniki pomiarów porowatości objętościowej dla badanego wzorca

Fig. 9. Histograms showing the numbers of pores with various sphericity coefficients for reconstructions with voxel sizes 15 μm, 30 μm and 65 μm
Rys. 9. Histogram przedstawiający liczbę porów o określonej sferyczności dla rekonstrukcji z wielkością woksela 15 μm, 30 μm i 65 μm
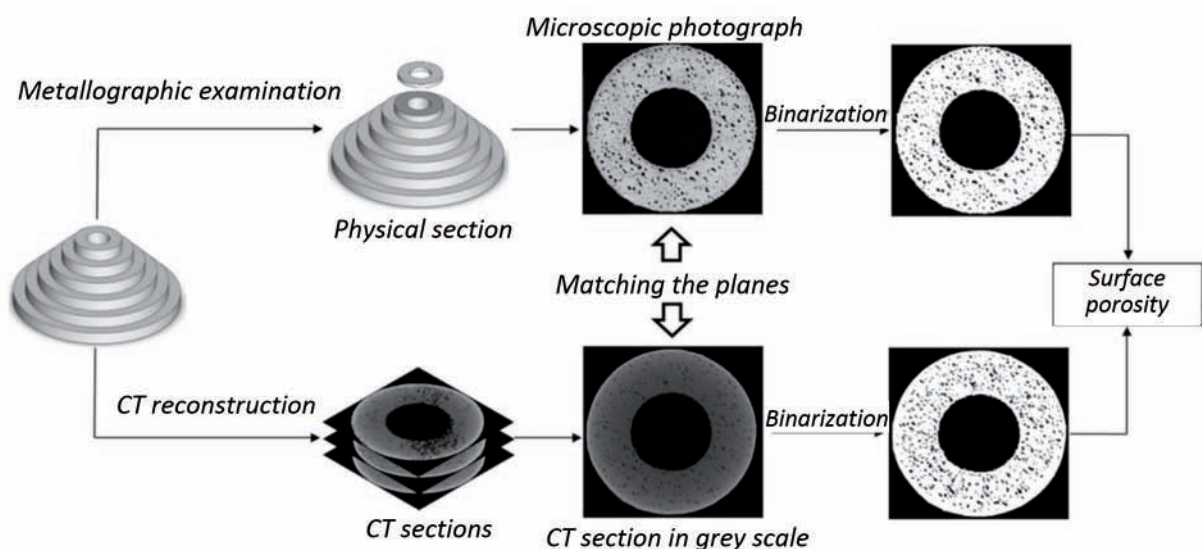

Fig. 10. Comparison of porosities determined by CT and on a metallographic polished section
Rys. 10. Schemat sposobu porównania przekrojów uzyskanych na zgładzie metalograficznym i na przekroju CT
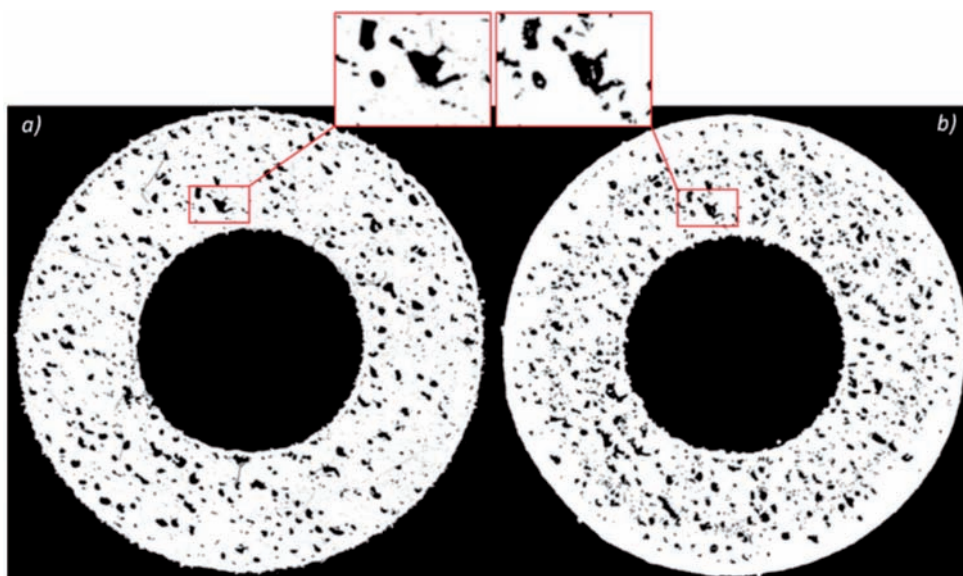

Fig. 11. Corresponding sections obtained by: a) microscopic examination; b) computed tomography
Rys 11. Odpowiadające przekroje: a) badaniu mikroskopowemu; b) tomografii komputerowej

microscopic measurements were compared. Porosity images after binarization, obtained for the metallographic section and CT section, are shown in Fig. 11.

In magnified fragments of the images, shapes and positions of pores recorded for both compared methods are visible. Differences in geometry of both magnified fragments are small. Differences in recorded pores outside of the indicated area may be due to the displacement of the plane of the metallographic section relative to the Z axis and the incomplete coverage of the comparable section. High accuracy of the performed reconstruction is confirmed by results of the determined porosity recorded by CT analysis. Surface porosity of the sample determined by microscopic observation was 8.22% and surface porosity of the same section, determined by CT, was 8.77%. This difference results, among others, from the fact that surfaces of pores are different in subsequent section planes of the object. Figure 12a shows a diagram of surface porosity recorded for CT sections between the planes A and B indicated in Fig. 12b. The distance between the planes was 2.2 mm and porosity was recorded on tomographic sections every 50 µm, see Fig. 12c.

It is visible on the sections that surface porosity depends on the location of the section between extreme planes A and B. For comparison, the value of surface porosity determined on one plane of the metallographic polished section is marked with red line. The differences in porosities recorded by microscopic examination and by CT result from cutting position and from selection of a representative plane for microscopic observation. In fact, porosity can be different depending on a given plane because of anisotropic arrangement or local accumulations of pores resulting from the manufacturing process, which significantly affects the final result of measurements.

4. Conclusions

The size of the sample determines the resolution of the measurement and the size of the voxel with which a CT reconstruction can be carried out, which significantly affects the sizes of recorded pores. Porosity recorded in the measurements taken with the highest ($V_x = 15$ µm) and the lowest ($V_x = 65$ µm) resolution was 8.33% and 4.02%, respectively. Images of pores recorded with larger voxels were more smoothed and closer to spherical shape. Comparative analysis recorded by microscopic observation and by CT (reconstruction with the highest resolution) showed similar values of surface porosity. Surface porosity determined by CT was 8.77%, but that determined in microscopic observation was 8.22%, so the difference did not exceed 1 percentage point. However, the most important benefit of CT measurements is the possibility of spatial representation of internal structure, which is a big advantage over traditional methods of porosity measurements, see Fig. 13.
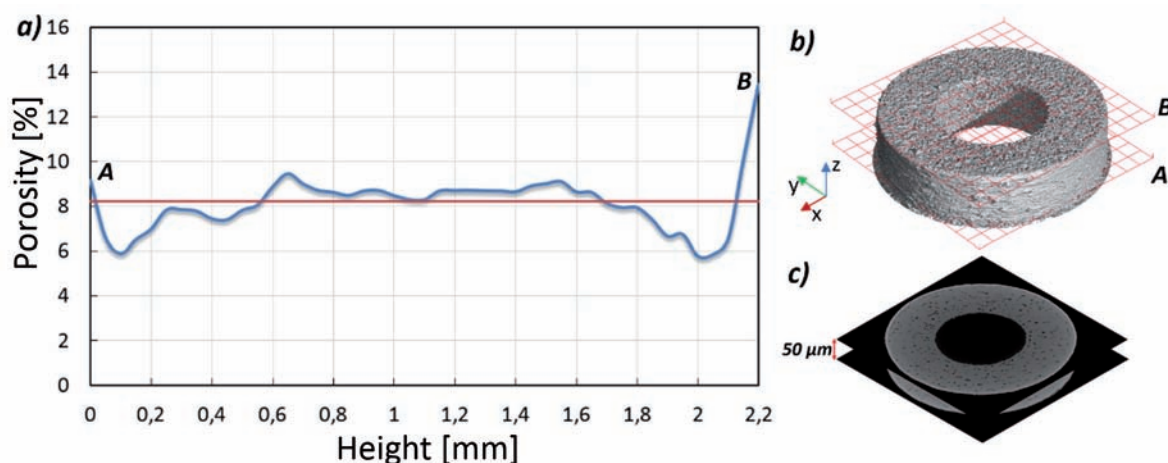

Fig. 12. Comparison of surface porosity PA measurements by CT and by microscopic observations: a) diagram of porosity in function of the location (height) of measured cross-sections between A and B planes (porosity determined by microscopic observation is marked by the red line); b) planes between that surface porosity was analysed; c) distance between tomographic sections for that porosity was determined
Rys. 12. Porównanie wyników pomiarów porowatości powierzchniowej PA metodą tomograficzną i mikroskopową: a) wykres przedstawiający zmiany porowatości w funkcji wysokości przekroju pomiędzy płaszczyznami A i B, (czerwoną linią zaznaczono porowatość zarejestrowaną za pomocą mikroskopu), b) płaszczyzny, pomiędzy którymi analizowano porowatość powierzchniową, c) odległość pomiędzy przekrojami tomograficznymi, dla których wyznaczono porowatość
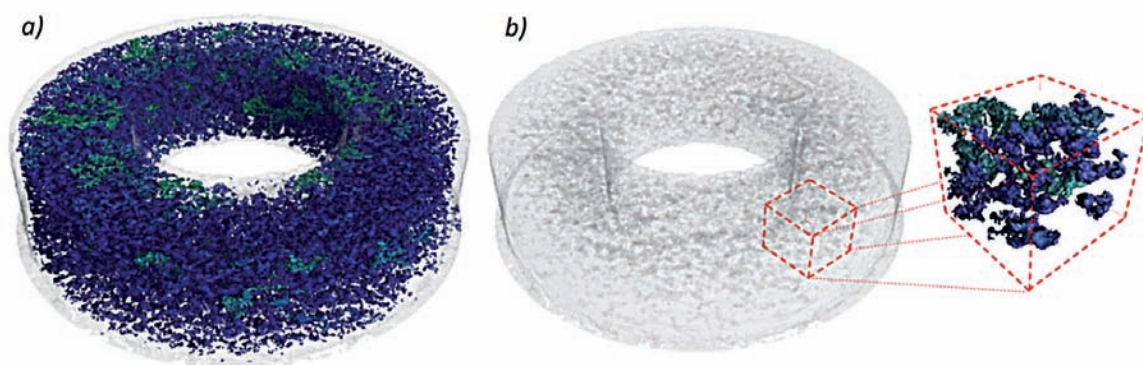

Fig. 13. Representation of three-dimensional internal structure of the examined object: a) global porosity; b) magnified fragment with marked local porosity
Rys. 13. Odwzorowanie trójwymiarowej struktury wewnętrznej badanego obiektu: a) porowatość globalna, b) powiększony fragment z zaznaczoną porowatością lokalną

Results of porosity recording with use of the CT technique for small-sized objects are comparable with those of standard microscopic examination. In case of larger objects, reconstruction with low resolution can be useful at identification of some characteristic areas, e.g. those with increased porosity. And for properly determined fragments of the object, exactness of reconstruction can be higher. Understanding the relations between the size of the object and the resolution of porosity measurement facilitates correct interpretation of results obtained by technical computed tomography.

References

1. Ratajczyk E., *X-ray computed tomography (CT) for industrial tasks.* "Pomiary Automatyka Robotyka". Vol. 16, No. 5, 2012, 104–113 (in Polish – *Rentgenowska tomografia komputerowa (CT) do zadań przemysłowych*).

2. Wieczorowski M., Gapiński B., *X-ray CT in metrology of geometric feature*, "Acta Tehnica Corviniensis – Bulletin of Engineering", Vol. 7, Iss. 1, 2014, 95–100.

3. Gapiński B., Wieczorowski M., Szymański M., Szymański S., Grzelka M., Rękas A., *Computed tomography in wall thickness measurements of profiles after bending.* "Mechanik". No. 11, 2016, 1712–1713, DOI: 10.17814/mechanik.2016.11.504 (in Polish – *Tomografia komputerowa w pomiarach grubości ścianek profili uzyskiwanych po gięciu*).

4. De Chiffre L., Carmignato S., Kruth J.-P., Schmitt R., Weckenmann A., *Industrial applications of computed tomography.* "CIRP Annals – Manufacturing Technology". Vol. 63, Iss. 2, 2014, 655–677, DOI: 10.1016/j.cirp.2014.05.011.

5. Probst G., Boeckmans B., Dewulf W., Kruth J.-P., *Computed tomography: a powerful imaging technique in the fields of dimensional metrology and quality control*, [in:] Proc. SPIE 9868, Dimensional Optical Metrology and Inspection for Practical Applications V, 98680G (May 19, 2016); DOI: 10.1117/12.2227146.

6. Królikowski M., Burbelko A., Kwaśniewska-Królikowska D., *Application of computed tomography in defectoscopy of nodular iron castings.* "Archives of Foundry Engineering", Vol. 14, Iss. 4, 2014, 71–76 (in Polish – *Wykorzystanie tomografii komputerowej w defektoskopii odlewów z żeliwa sferoidalnego*).

7. Dybała B., Będza T., Ziółkowski G., *Technical computed tomography in metrology of geometrical quantities and quality inspection.* "Mechanik". Vol. 86, No. 7, 2013, 526–530 (in Polish – *Techniczna tomografia komputerowa w metrologii wielkości geometrycznych i kontroli jakości*).

8. Chlebus E., Ziółkowski G., Dybała B., *Application of industrial computed tomography in assembly analysis.* "Mechanik". Vol. 86, No. 5–6, 2013, 422–424, 426 (in Polish – *Zastosowanie przemysłowej tomografii komputerowej w analizie złożeń*).

9. Kumar J., Abulrub A.G., Attridge A., Williams M.A., *Effect of X-Ray Computed Tomography Scanning Parameters on the Estimated Porosity of Foam Specimens.* 2nd International Conference on Mechanical, Industrial, and Manufacturing Technologies (MIMT 2011).

10. Stock S R., *Microcomputed Tomography – Methodology and Application.* CRC Press, Boca Raton 2009.

11. Ketcham R.A., Hanna R.D., *Beam hardening correction for X-ray computed tomography of heterogeneous natural materials*, "Computers & Geosciences". Vol. 67, 2014, 49–61, DOI: 10.1016/j.cageo.2014.03.003.

12. Schörner K., Goldammer M., Stephan J., *Comparison between beam-stop and beam-hole array scatter correction*, "Nuclear Instruments and Methods in Physics Research B". Vol. 269, Iss. 3, 2011, 292–299, DOI: 10.1016/j.nimb.2010.11.053.

13. Iassonov P., Gebrenegus T., Tuller M., *Segmentation of X-ray computed tomography images of porous materials: A crucial step for characterization and quantitative analysis of pore structures.* "Water Resources Research", Vol. 45, Iss. 9, 2009, DOI: 10.1029/2009WR008087.

14. Wu J., Li X., Wang Y., Zhang B., *An Improved Algorithm in Porosity Characteristics Analysis for Rock and Soil Aggregate*, "Discrete Dynamics in Nature and Society". Vol. 2014, DOI: 10.1155/2014/798235.

15. Ziółkowski G., Chlebus E., Szymczyk P., Kurzac J., *Application of X-ray CT method for discontinuity and porosity detection in 316L stainless steel parts produced with SLM technology.* "Archives of Civil and Mechanical Engineering". Vol. 14, Iss. 4, 2014, 608–614,
DOI: 10.1016/j.acme.2014.02.003.

Detekcja porowatości z wykorzystaniem technicznej tomografii komputerowej

Streszczenie: Techniczna tomografia komputerowa CT (ang. Computed Tomography) wspomaga kontrolę jakości wytwarzanych obiektów technicznych i rozwój produktu dzięki możliwości nieniszczącej detekcji porowatości. Wykorzystanie tomografii komputerowej w defektoskopii pozwala nie tylko na jakościową ocenę struktury wewnętrznej obiektów, ale i na ilościową ocenę porowatości ich materiału z odwzorowaniem trójwymiarowego kształtu porów i ich rozkładu przestrzennego. W pracy przedstawiono krótką charakterystykę czynników wpływających na skuteczność detekcji porowatości z wykorzystaniem metody CT. Na przykładzie obiektu technicznego przedstawiono wpływ zastosowanego powiększenia na możliwości detekcji porowatości i odwzorowania kształtu porów. Następnie porównano wyniki porowatości uzyskanej z wykorzystaniem metody CT i standardowych badań mikroskopowych. Wykazano wpływ powiększenia i rozdzielczości pomiaru na możliwość detekcji porów z wykorzystaniem metody CT.

Słowa kluczowe: techniczna tomografia komputerowa, porowatość, defektoskopia, kontrola jakości

Grzegorz Ziółkowski, PhD
grzegorz.ziolkowski@pwr.edu.pl

Received his PhD (2016) degree from the Wrocław University of Science and Technology. He is an assistant professor at the Faculty of Mechanical Engineering of WrUST. His current research interests include non-destructive testing especially computed tomography, quality control for parts produced by additive technology, reverse engineering, CAD design and FEM analysis.

Patrycja Szymczyk, PhD
patrycja.e.szymczyk@pwr.edu.pl

Received her PhD (2015) degree from the Wrocław University of Science and Technology. She is an assistant professor at the Faculty of Mechanical Engineering of WrUST. Her current research interests include materials engineering, materials testing and additive manufacturing technologies (SLM/DMLS, EBM, FDM, 3DP), especially for biomedical applications.

Andrzej Pawlak, MSc
andrzej.p.pawlak@pwr.edu.pl

Received his MSc (2011) degree from Wrocław University of Science and Technology. He is currently a PhD student at the Faculty of Mechanical Engineering of WrUST. Within the PhD he deals with the optimisation of process parameters of magnesium alloy powders manufactured using selective laser melting method.

Tomasz Kurzynowski, PhD
tomasz.kurzynowski@pwr.edu.pl

Received his PhD (2011) degree from the Wrocław University of Science and Technology. He is assistant professor at the Faculty of Mechanical Engineering of WrUST. His current research interests include additive manufacturing technologies and design methods for functional optimization or weight reduction of designed or reengineered parts, especially for the aerospace industry.

Bogdan Dybała, PhD DSc
bogdan.dybala@pwr.wroc.pl

Received his DSc (habilitation, 2014) degree from the Wrocław University of Science and Technology. He is s currently an associate professor at the Faculty of Mechanical Engineering of WrUST. His current research interests include additive manufacturing technologies and reverse engineering, with special focus on their biomedical applications.

Professor Edward Chlebus, PhD DSc
edward.chlebus@pwr.edu.pl

Received his PhD (1972) and DSc (1993) degrees from the Wrocław University of Science and Technology. Since 2001 he is the Professor of technical sciences. He is the director of the Centre for Advanced Manufacturing Technologies and the Fraunhofer Project Center for Laser Integrated Manufacturing (CAMT-FPC) at the Faculty of Mechanical Engineering of WrUST. His current research interest include: design, CAx techniques – design methodology issues, with particular emphasis on computer-aided engineering, product development and additive manufacturing.